

Sites and dynamics of hydrogen and deuterium in V-H-D alloys studied by ^1H and ^2H NMR

Bilwadal Bandyopadhyay* and Shigenobu Hayashi†

National Institute of Materials and Chemical Research, 1-1 Higashi, Tsukuba, Ibaraki 305-8565, Japan

(Received 26 February 1999; revised manuscript received 2 June 1999)

Vanadium-hydrogen-deuterium (V-H-D) alloys with $([\text{H}]+[\text{D}])/[\text{V}]=0.8$ have been studied by means of x-ray diffraction, thermal analysis, and ^1H and ^2H NMR. The crystal structures of $\text{VH}_{0.82}$ and $\text{VH}_{0.6}\text{D}_{0.2}$ are body-centered-tetragonal (bct), while those of $\text{VH}_{0.2}\text{D}_{0.6}$ and $\text{VD}_{0.81}$ are body-centered-cubic (bcc). $\text{VH}_{0.4}\text{D}_{0.4}$ consists of bct and bcc, demonstrating the existence of an immiscibility region. The phase transition from the δ_{D} phase to the α_{D} phase is observed in $\text{VD}_{0.81}$ between 200 and 240 K. The temperature range of the similar phase transition becomes broadened and shifted toward the lower temperature as the $[\text{H}]/[\text{D}]$ ratio increases. In $\text{VH}_{0.82}$ no phase transition is observed in the temperature range between 120 and 295 K. In $\text{VH}_{0.81}$, H atoms occupy octahedral (O) sites, and H diffusion takes place between the ordered O sites. In $\text{VH}_{0.6}\text{D}_{0.2}$, H and D atoms occupy both the O and tetrahedral (T) sites, and the H and D atoms in the T sites diffuse faster than those in the O sites do. The diffusion between the ordered O sites is confirmed by the residual ^1H dipolar broadening and the ^2H quadrupolar line shape. In $\text{VH}_{0.2}\text{D}_{0.6}$ and $\text{VD}_{0.81}$, H and D atoms occupy the T sites. In the δ_{D} phase H and D atoms diffuse among the ordered T sites, and consequently the ^2H quadrupolar line shape is preserved and the ^2H relaxation is caused dominantly by the dipolar interaction. Around the phase transition temperature range, the diffusion changes drastically. In the α_{D} phase the diffusion takes place between the disordered T sites, and another motional mode is additionally present. Temperature and frequency dependences of ^1H and ^2H spin-lattice relaxation times can be described by modified Bloembergen-Purcell-Pound equations, suggesting that H and D atoms undergo some kind of correlated motions. Activation energies and mean residence times of H and D atoms have been estimated for each site. [S0163-1829(99)11137-8]

I. INTRODUCTION

Vanadium (V) metal can absorb a large amount of hydrogen to the extent of a hydrogen-to-metal ratio of 2.¹ The structures and phase diagrams of vanadium hydrides and vanadium deuterides have been extensively studied in the past.² It is known that hydrogen (H) and deuterium (D) atoms occupy different sites in the monohydride (or monodeuteride) of vanadium, leading to much different phase diagrams between the V-H and V-D systems. For example, at room temperature, $\text{VH}_{0.8}$ has a body-centered-tetragonal (bct) structure with H atoms occupying octahedral (O) sites, which is referred as the ζ_{H} phase. On the other hand, $\text{VD}_{0.8}$ has a body-centered-cubic (bcc) structure in which D atoms mostly occupy tetrahedral (T) sites. In the deuteride, the interstitial D atoms form an ordered orthorhombic sublattice below about 230 K. Above 230 K, the D atoms distribute randomly. The phases are denoted as δ_{D} and α_{D} below and above 230 K, respectively.

NMR is useful to study hydrogen diffusion in metal hydrides.³ Fukai and Kazama have studied hydrogen diffusion in VH_x ($0.49 \leq x \leq 0.74$) by ^1H NMR.⁴ The observed anomalous temperature dependence of ^1H spin-lattice relaxation time (T_1) was explained as a consequence of temperature-dependent activation energy of hydrogen diffusion. We have studied hydrogen diffusion in $\text{VH}_{0.59}$ and $\text{VH}_{0.77}$, relating it to the superstructures of H atoms.^{5,6}

When the concentration of solute atoms is very low, H atoms diffuse faster than D atoms in vanadium.⁷ Salibi *et al.* have studied vanadium, niobium, and tantalum deuterides by ^2H NMR.⁸ The results of $\text{VD}_{0.59}$ were complicated, and thus further measurements were necessary to elucidate the deute-

rium diffusion at this deuterium concentration. In our previous work, we have studied the isotope effect on hydrogen diffusion in Ti-V-H systems.^{9,10} The monohydride and monodeuteride have the same crystal structure, and the apparent activation energies for hydrogen diffusion were found to be larger than those for deuterium diffusion.

There may be interaction between diffusing atoms at high concentration of diffusing atoms. Fukai, Kubo, and Kazama have studied hydrogen diffusion in $\alpha\text{-NbH}_x\text{D}_y$ by a pulsed-field-gradient spin-echo NMR technique.¹¹ They found the lowering of H diffusion coefficient in the range of $x < 0.1$ only for the samples with $x + y \leq 0.60$. The sample with $x + y = 0.75$ showed no dependence on the $[\text{H}]/[\text{D}]$ ratio. To our knowledge, no other reports have been published for the systems containing both H and D.

In the present work, we have studied V-H-D systems with the $([\text{H}]+[\text{D}])/[\text{V}]$ ratio of 0.8. $\text{VH}_{0.8}$ and $\text{VD}_{0.8}$ have different crystal structures, as described above. The site occupancies, the diffusions of hydrogen and deuterium, and furthermore, the crystal structures are expected to depend on the $[\text{H}]/[\text{D}]$ ratio. NMR techniques are suitable for this work, because hydrogen and deuterium can be completely separated in the observations of ^1H and ^2H NMR even when they are mixed. We report the results of ^1H and ^2H NMR measurements on VH_xD_y ($x + y = 0.8$) as well as $\text{VH}_{0.82}$ and $\text{VD}_{0.81}$, and discuss on the sites and diffusions of hydrogen and deuterium.

II. EXPERIMENT

A. Materials

Vanadium metal powder (200 mesh, 99.5% min.) was obtained from Mitsuwa Pure Chemicals (Japan). The hydride

($\text{VH}_{0.82}$) and the deuteride ($\text{VD}_{0.81}$) were prepared by a reaction between vanadium metal and H_2 (or D_2) gas at pressures less than 1 atm. The metal was first outgassed at 873 K and then held at 673 K, where H_2 (or D_2) gas was introduced. The temperature of the reaction was brought down to ambient temperature slowly over a day. The H (or D) content was estimated by a volumetric method. In order to obtain the VH_xD_y alloys as hydrogen-rich $\text{VH}_{0.60}\text{D}_{0.20}$, deuterium-rich $\text{VH}_{0.20}\text{D}_{0.60}$ and $\text{VH}_{0.40}\text{D}_{0.40}$ (equal amounts of hydrogen and deuterium), the pure hydride ($\text{VH}_{0.82}$) and the pure deuteride ($\text{VD}_{0.81}$) were mixed in appropriate ratios and homogenized inside a closed chamber at 573 K for one week. Approximately 30% of the gas components (H and D) evolved during each homogenization, and during subsequent cooling all except about 4% of the gas components was reabsorbed. Since the amount of the leftover gas was nearly equivalent to the maximum error, ± 0.02 , in our estimation of H (or D) concentration, the desired VH_xD_y alloys were obtained. For simplicity, the compositions are expressed as $\text{VH}_{0.6}\text{D}_{0.2}$, $\text{VH}_{0.2}\text{D}_{0.6}$, and $\text{VH}_{0.4}\text{D}_{0.4}$.

B. X-ray diffraction and thermal analysis

X-ray powder diffraction patterns were measured by a Rigaku RAX-01 Geiger Flex diffractometer with Cu $K\alpha$ radiation at room temperature. Differential scanning calorimetric (DSC) measurements were carried out in the temperature range between 120 and 295 K using a Rigaku DSC8230 combined with a thermal analysis station TAS100. The sample temperature was raised at a rate of 5 K/min under nitrogen gas flow.

C. ^1H NMR measurements

The ^1H NMR measurements have been performed by a Bruker CXP90 spectrometer equipped with a Tecmag Real-time NMR Station MiniMacSpect operated by MacNMR5.3 software. The magnetic field was provided by a Bruker current controlled electromagnet, and Larmor frequencies were set at 30.3 and 59.8 MHz. The stability of the magnetic field was not very good, and then the signal position was adjusted to the center of the spectrum in each experiment. A Bruker BVT1000 temperature controller was used to vary the temperature of the sample in the range between 110 and 420 K. The measurements at 77 K were done by putting the sample in a liquid nitrogen dewar inserted in the NMR probehead.

The 90° pulse width for ^1H was less than $5 \mu\text{s}$, which was determined for the samples themselves. Both the ordinary inversion recovery pulse sequence ($180^\circ-\tau-90^\circ$) and that followed by the solid echo pulse sequence ($180^\circ-\tau-90^\circ_x-\tau_1-90^\circ_y-\tau_2$ -echo) were used for most of the T_1 measurements. In these pulse sequences, τ denotes the variable delay time. For the T_1 measurements at low temperatures where there was a large broadening of the spectra, the magnetization was first saturated by a string of near 90° pulses, and then its recovery with time was monitored. The pulse sequence was $n90^\circ-\tau-90^\circ_x-\tau_1-90^\circ_y-\tau_2$ -echo. The quadrature mode of detection was used throughout.

D. ^2H NMR measurements

The ^2H NMR measurements have been performed by Bruker ASX200 and MSL400 NMR spectrometers, and the

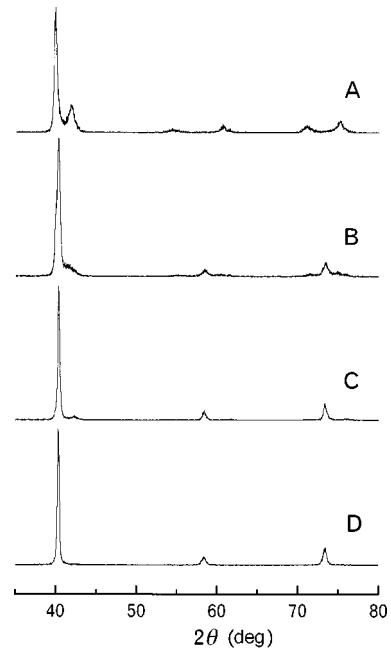


FIG. 1. X-ray powder-diffraction patterns of (A) $\text{VH}_{0.6}\text{D}_{0.2}$, (B) $\text{VH}_{0.4}\text{D}_{0.4}$, (C) $\text{VH}_{0.2}\text{D}_{0.6}$, and (D) $\text{VD}_{0.81}$ at room temperature.

respective fixed-field superconducting magnets were used. Larmor frequencies were 30.7 and 61.4 MHz, respectively. The temperature was varied by Bruker temperature controllers in the range between 140 and 420 K.

The 90° pulse widths for ^2H were between 2.5 and $5 \mu\text{s}$ and between 5 and $10 \mu\text{s}$ for ASX200 and MSL400, respectively, which were determined for each sample. The spectra were measured with the quadrupole echo pulse sequence ($90^\circ_x-\tau_1-90^\circ_y-\tau_2$ -echo). The τ_1 was set at $15 \mu\text{s}$, and the τ_2 value was adjusted to the echo maximum. The spectra were expressed with the signal of D_2O being 0 Hz. The three pulse sequences used for the ^1H T_1 measurements were also used for the ^2H T_1 measurements.

III. RESULTS AND DISCUSSION

A. X-ray diffraction

The x-ray powder-diffraction patterns of the VH_xD_y alloys together with that of $\text{VD}_{0.81}$ are shown in Fig. 1. $\text{VH}_{0.82}$ shows a pattern almost identical with that of $\text{VH}_{0.6}\text{D}_{0.2}$. The crystal structure and lattice constants are listed in Table I. $\text{VH}_{0.82}$ has a bct structure with lattice constants of $a = 0.303 \text{ nm}$ and $c = 0.340 \text{ nm}$. The c/a ratio is 1.12. The H atoms occupy the O sites.² The hydrogen-rich $\text{VH}_{0.6}\text{D}_{0.2}$ has also the bct structure with $a = 0.305 \text{ nm}$ and $c = 0.333 \text{ nm}$. The reduced value of c ($c/a = 1.09$) suggests that unlike the pure hydride, the H and/or D atoms in $\text{VH}_{0.6}\text{D}_{0.2}$ occupy not only the O sites but also the T sites. $\text{VD}_{0.81}$ has a bcc structure with $a = 0.316 \text{ nm}$. The x-ray-diffraction pattern of the deuterium-rich $\text{VH}_{0.2}\text{D}_{0.6}$ shows that this alloy forms predominantly the bcc structure ($a = 0.316 \text{ nm}$) similar to the pure deuteride, but the presence of a small amount of the bct phase is also indicated. However, $\text{VH}_{0.4}\text{D}_{0.4}$ is clearly a mixed-phase alloy containing both the bct and bcc phases.

TABLE I. Crystal structures and calculated second moments for ^1H and ^2H .

Sample	Crystal structure	H/D site	M_{HH} (kHz) ²	M_{HV} (kHz) ²	M_{DH} (kHz) ²	M_{DV} (kHz) ²
VH _{0.82}	bct $a = 0.303$ nm $c = 0.340$ nm	<i>O</i>	162.4	614.6	---	---
VH _{0.6} D _{0.2}	bct $a = 0.305$ nm $c = 0.333$ nm	<i>O</i> <i>T</i>	118.9 108.8	612.8 656.3	1.2 1.1	14.4 15.5
VH _{0.2} D _{0.6}	bcc $a = 0.316$ nm	<i>T</i>	34.4	626.6	0.3	14.8
VD _{0.81}	bcc $a = 0.316$ nm	<i>T</i>	---	---	0	14.8

In conclusion, the $[\text{H}]/[\text{D}]$ ratio cannot be changed continuously in VH_xD_y ($x+y=0.8$). There exists an immiscibility gap in the region of about equal concentrations of H and D.

B. DSC

The results of the DSC measurements are shown in Fig. 2. In VD_{0.81}, as the temperature increases, an endothermic peak starts to develop at near 200 K and ends at about 240 K. As previously mentioned, vanadium deuteride with this composition undergoes a transition from the δ_{D} phase to the α_{D} phase at about 230 K.² In the δ_{D} phase the D atoms form a partially ordered structure, and by that transition the ordering disappears. The peak becomes broadened and shifted toward the lower temperature as the $[\text{H}]/[\text{D}]$ ratio increases. In VH_{0.2}D_{0.6}, the peak is distributed over the range between 190 and 235 K, and has a shoulder in the low-temperature side. Interestingly, only in this sample there is an additional small peak centered at about 140 K and finishing at 148 K. In the

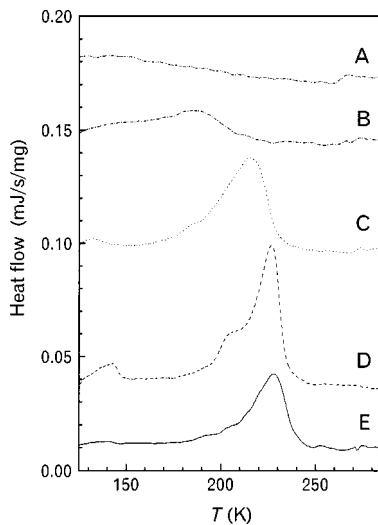


FIG. 2. DSC curves for (A) VH_{0.82}, (B) VH_{0.6}D_{0.2}, (C) VH_{0.4}D_{0.4}, (D) VH_{0.2}D_{0.6}, and (E) VD_{0.81}. Heat absorption is expressed as the positive direction. The magnitudes of the heat flow are normalized by the sample weight, and the zero positions are shifted by arbitrary amounts.

deuteride, the γ_{D} phase with a fully ordered D lattice coexists with the δ_{D} phase below 135 K.² However, no signature of this transition could be obtained in the DSC measurement on VD_{0.81}. Consequently, the small peak at 140 K in VH_{0.2}D_{0.6} might indicate an ordering of H atoms, which in this case is facilitated by the presence of D atoms in high concentration. In VH_{0.4}D_{0.4}, the main peak is further broadened and shifted. This means that VH_{0.4}D_{0.4} is not a mixture of VH_{0.2}D_{0.6} and VH_{0.6}D_{0.2}. In other words, the immiscibility gap is smaller than the range covering VH_{0.2}D_{0.6} and VH_{0.6}D_{0.2}. In VH_{0.6}D_{0.2}, the peak starts to develop at the lowest temperature observed and is distributed up to about 215 K. VH_{0.82} does not show any indication of a peak in the temperature range studied. The DSC results obtained indicate that D atoms tend to be ordered and that the presence of H atoms hinders the D ordering.

C. ^1H NMR spectra

^1H NMR spectra have been measured for VH_xD_y and VH_{0.82} alloys at 30.3 and 59.8 MHz in the temperature range between 110 and 420 K. In VH_{0.82} and VH_{0.2}D_{0.6}, the spectra at any temperatures can apparently be fitted with a single Lorentzian line shape. However, in VH_{0.6}D_{0.2}, the spectra clearly show a superposition of two components with different linewidths below 150 K, as shown in Fig. 3. This fact suggests that H atoms occupy two different sites with different motional properties in VH_{0.6}D_{0.2}. Since the dipolarly broadened line shape is Gaussian-like, Lorentzian line shapes in VH_{0.82} and VH_{0.2}D_{0.6} at low temperatures might mean the existence of two components.

Figures 4 and 5 show the temperature dependence of the full width at half maximum (FWHM) at both 30.3 and 59.8 MHz. The characteristic ‘‘motional narrowing’’ of the ^1H resonance line is observed in all the samples. In VH_{0.82} the motional narrowing is completed at about 210 K. In the high-temperature range the linewidth is about 15 and 18 kHz at 30.3 and 59.8 MHz, respectively. The dipole-dipole interaction, which is field-independent, has a dominant contribution to the linewidth even in the high-temperature range. This fact means that the hydrogen diffusion is not isotropic but rather

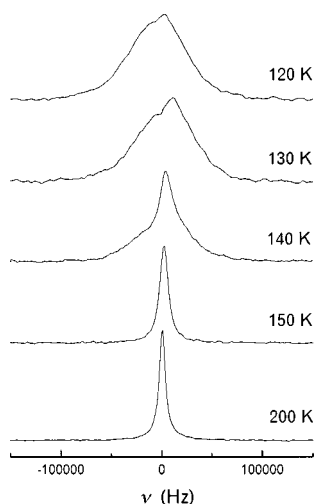


FIG. 3. Temperature dependence of ^1H NMR spectra of $\text{VH}_{0.6}\text{D}_{0.2}$, measured at 30.3 MHz. The position is not very accurate due to the limited stability of the electromagnet used. The 0-Hz position is approximately the signal of H_2O .

anisotropic. In $\text{VH}_{0.2}\text{D}_{0.6}$ the motional narrowing is almost completed at about 160 K, much lower than that in $\text{VH}_{0.82}$, demonstrating that hydrogen diffusion is faster in $\text{VH}_{0.2}\text{D}_{0.6}$ than in $\text{VH}_{0.82}$. At the high-temperature side the residual linewidth is much smaller than that in $\text{VH}_{0.82}$ and is proportional to the applied static magnetic field. The dipole-dipole interaction is averaged out, and the bulk magnetization contributes to the linewidth. Hydrogen diffusion is considered to be isotropic in $\text{VH}_{0.2}\text{D}_{0.6}$.

In $\text{VH}_{0.6}\text{D}_{0.2}$, since two components with different linewidths are superposed below 150 K, the linewidths are plotted only at and above 150 K in Fig. 5. The figure shows clearly humps near 200 K. This indicates that at least two components undergo independent motional narrowing in certain temperature ranges. The motional narrowing is almost completed at about 160 and 240 K, respectively. This might

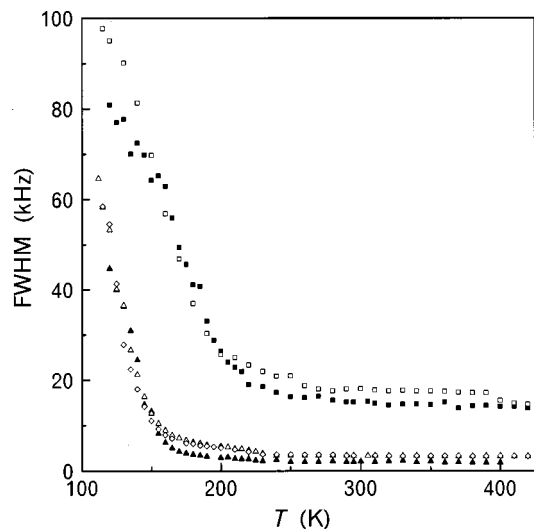


FIG. 4. Temperature dependence of ^1H NMR linewidths in ■: $\text{VH}_{0.82}$ at 30.3 MHz, □: $\text{VH}_{0.82}$ at 59.8 MHz, ▲: $\text{VH}_{0.2}\text{D}_{0.6}$ at 30.3 MHz, △: $\text{VH}_{0.2}\text{D}_{0.6}$ at 59.8 MHz, and ◇: $\text{VH}_{0.4}\text{D}_{0.4}$ at 59.8 MHz. Above 200 K, △ is hidden behind ◇.

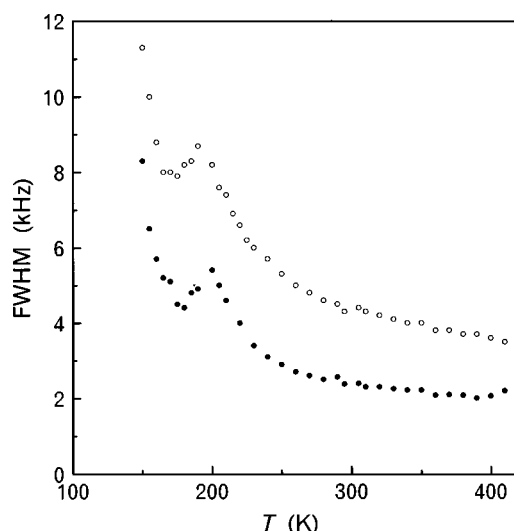


FIG. 5. Temperature dependence of ^1H NMR linewidths in $\text{VH}_{0.6}\text{D}_{0.2}$, measured at 30.3 (●) and 59.8 MHz (○).

arise from H atoms occupying different types of sites wherein they have different mobilities. Above 240 K, the line width in $\text{VH}_{0.6}\text{D}_{0.2}$, which is broader than that in $\text{VH}_{0.2}\text{D}_{0.6}$, gradually decreases and reaches to the width of $\text{VH}_{0.2}\text{D}_{0.6}$ at 400 K. The residual dipole-dipole interaction remains in $\text{VH}_{0.6}\text{D}_{0.2}$ below 400 K.

Figure 4 includes also the results of $\text{VH}_{0.4}\text{D}_{0.4}$ at 59.8 MHz, although the sample is a mixed-phase one. The linewidths of $\text{VH}_{0.4}\text{D}_{0.4}$ agree with those of $\text{VH}_{0.2}\text{D}_{0.6}$. The fraction of the bcc phase might be larger than that of bct in this sample.

D. ^1H spin-lattice relaxation time

^1H spin-lattice relaxation times have been measured for VH_xD_y and $\text{VH}_{0.82}$ alloys at 30.3 and 59.8 MHz in the temperature range between 77 and 420 K. The recovery of the ^1H magnetization is found to be exponential in all the samples at 77 K. At this temperature, the ^1H T_1 values are 2.01 ± 0.17 , 2.36 ± 0.27 , and 2.65 ± 0.30 s for $\text{VH}_{0.82}$, $\text{VH}_{0.6}\text{D}_{0.2}$, and $\text{VH}_{0.2}\text{D}_{0.6}$, respectively. They agree with each other at the two Larmor frequencies within experimental errors. In the temperature range between 110 and 420 K, the recovery is sometimes nonexponential. The experimentally obtained T_1 of ^1H in VH_xD_y and $\text{VH}_{0.82}$ at 59.8 MHz are plotted as a function of inverse temperature in Figs. 6 and 7, except for the values at 77 K.

In $\text{VH}_{0.82}$ and $\text{VH}_{0.2}\text{D}_{0.6}$ the deviations from single exponential behavior are noticeable in the recovery of ^1H magnetization only at 30.3 MHz, in $\text{VH}_{0.82}$ the deviation occurs in the low end of the temperature range, and in $\text{VH}_{0.2}\text{D}_{0.6}$ it occurs both in the low and the high ends of the temperature range. The same samples, when measured at 59.8 MHz, show negligible deviations from single exponential behavior. In $\text{VH}_{0.82}$ and $\text{VH}_{0.2}\text{D}_{0.6}$, therefore, we have obtained and analyzed the apparent single exponent relaxation time, i.e., the time in which the magnetization recovery reaches $1/e$ of its initial value.

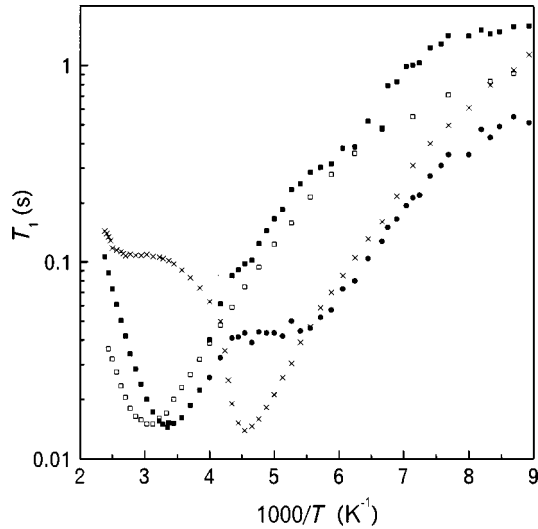


FIG. 6. Temperature dependence of ^1H spin-lattice relaxation times at 59.8 MHz. \square : $\text{VH}_{0.82}$, \blacksquare : component 1 in $\text{VH}_{0.6}\text{D}_{0.2}$, \bullet : component 2 in $\text{VH}_{0.6}\text{D}_{0.2}$, and \times : $\text{VH}_{0.2}\text{D}_{0.6}$.

In $\text{VH}_{0.82}$, T_1 yields a minimum of 8.0 ms at 310 K when observed at 30.3 MHz, whereas at 59.8 MHz the minimum is 15 ms at 325 K. With the increase in Larmor frequency, the minimum value increases and its position shifts to the higher temperature direction. The shape of the T_1 versus T^{-1} plot is asymmetric with respect to the temperature of the minimum point.

The T_1 of ^1H in the deuterium-rich $\text{VH}_{0.2}\text{D}_{0.6}$ yields a minimum of 6.7 ms at 215 K and 30.3 MHz. The minimum is 13.9 ms at 220 K when measured at 59.8 MHz. The temperature of the minimum point is not very much shifted with Larmor frequency. In this sample, the order-disorder transition of the D sublattice takes place below 235 K, as has been indicated by the DSC experiment. The T_1 behavior around the transition temperature indicates an abrupt change in hydrogen motion.

In the hydrogen-rich $\text{VH}_{0.6}\text{D}_{0.2}$, the recovery curve observed at both 30.3 and 59.8 MHz can be expressed as a sum

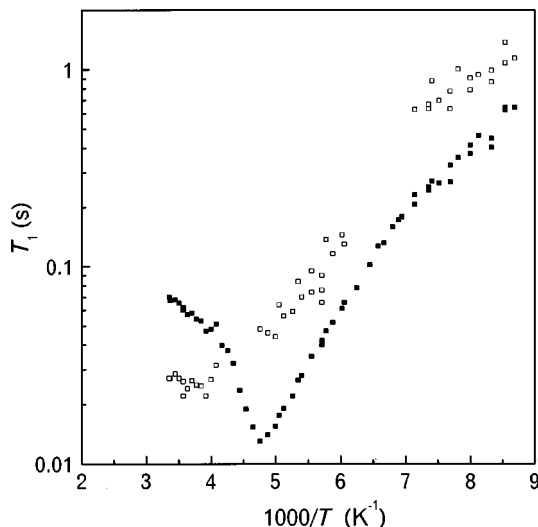


FIG. 7. Temperature dependence of ^1H spin-lattice relaxation times in $\text{VH}_{0.4}\text{D}_{0.4}$ at 59.8 MHz. \square : component 1 and \blacksquare : component 2.

of two exponents of significant magnitudes below about 225 K, showing the presence of H atoms in two types of environments. Above this temperature the recovery is single exponential. The longer T_1 component below 225 K connects smoothly with the single T_1 value above this temperature, and their temperature dependence is similar to that in $\text{VH}_{0.82}$. The minimum values are 7.7 ms (280 K) and 14.4 ms (298 K) at 30.3 and 59.8 MHz, respectively. The shorter T_1 component follows the behavior in the deuterium-rich sample $\text{VH}_{0.2}\text{D}_{0.6}$ at low temperatures.

The recovery curves in $\text{VH}_{0.4}\text{D}_{0.4}$ show nonexponential behavior, being composed of two components. Figure 7 shows ^1H T_1 values measured at 59.8 MHz. While the recovery curves were measured in the temperature range between 115 and 298 K, the second T_1 values are missing between 144 and 160 K and between 215 and 240 K, as the nonexponentiality is very small in those temperature ranges. The temperature dependence of the component 1 (\square) resembles the average values in $\text{VH}_{0.6}\text{D}_{0.2}$, whereas the component 2 (\blacksquare) shows dependence similar to that of $\text{VH}_{0.2}\text{D}_{0.6}$ with a minimum of 13 ms (210 K). These results reflect the presence of two phases in this sample.

E. Analysis of ^1H spin-lattice relaxation time

For a nucleus with spin $I = \frac{1}{2}$ in metal hydrides, the spin-lattice relaxation rate can be expressed as

$$(T_1)^{-1} = (T_{1d})^{-1} + (T_{1e})^{-1} + (T_{1p})^{-1}, \quad (1)$$

where $(T_{1d})^{-1}$ is contribution from modulation of nuclear dipolar interactions, $(T_{1e})^{-1}$ arises from fluctuation of hyperfine interaction between the nuclear spin and conduction electrons, and $(T_{1p})^{-1}$ is contribution from the dipolar interaction between the nuclear spin and electron spins on paramagnetic impurities. The temperature dependence of T_{1e} is given by Korringa relation, $T_{1e}T = \text{constant}$.

At low temperatures where hydrogen diffusion is sufficiently slowed down, $(T_{1d})^{-1}$ is negligible. Assuming that the contribution from $(T_{1p})^{-1}$ can be ignored, only $(T_{1e})^{-1}$ becomes significant. Korringa constants $T_{1e}T$ for ^1H are estimated from the T_1 values at 77 K, which are listed in Table II. Fukai and Kazama adopted a value of 102 s K for $\text{VH}_{0.736}$, which was estimated from T_1 data at low temperatures as low as 93 K.⁴ In the same paper, they adopted values of 119, 113, and 135 s K for $\text{VH}_{0.486}$, $\text{VH}_{0.546}$, and $\text{VH}_{0.622}$, respectively. In a separate paper, they reported $T_{1e}T$ values in the α_{H} phase of vanadium hydrides, which are 133 s K for $\text{VH}_{0.736}$.¹² In consideration of those results, the obtained value for $\text{VH}_{0.82}$ (155 s K) is reasonable, and the contribution from paramagnetic impurities can be neglected. With decrease in the $[\text{H}]/[\text{D}]$ ratio, there might be a genuine increase in Korringa constant, which might correlate with the structure change from bct to bcc.

The dipolar relaxation times T_{1d} are obtained by removing the contribution of T_{1e} , which are plotted in Figs. 8–10 and used to evaluate parameters relating to hydrogen diffusion. The dipolar contribution in Eq. (1) is written as

$$(T_{1d})^{-1} = (T_{1d})_{\text{HH}}^{-1} + (T_{1d})_{\text{HV}}^{-1}. \quad (2)$$

TABLE II. ^1H Korringa constants and parameters of hydrogen diffusion.

Sample	$T_{1e}T$ (s K)	H site	$\tau_{0\text{H}}^{\text{a}}$ (s)	E_{H} (eV/atom)	α	f_1
VH _{0.82}	155 ± 13	<i>O</i>	9×10^{-14}	0.315	0.35	0.35
VH _{0.6} D _{0.2}	182 ± 21	<i>O</i>	9×10^{-14}	0.277	0.55	0.40
		<i>T</i>	3×10^{-14}	0.20	0.48	0.15
VH _{0.2} D _{0.6}	204 ± 23	<i>T</i> ^b	3×10^{-14}	0.23	0.53	0.45
		<i>T</i> ^c	3×10^{-14}	0.195	0.53 ^a	0.45 ^a
		<i>O'</i> ^c	9×10^{-14}	0.36	0.20	0.035

^aAssumed.^bBelow 220 K.^cAbove 240 K.

$(T_{1d})_{\text{HH}}^{-1}$ and $(T_{1d})_{\text{HV}}^{-1}$ are the contributions from the modulation of nuclear dipolar interactions between ^1H spins and between ^1H and ^{51}V spins, respectively. $(T_{1d})_{\text{HH}}^{-1}$ and $(T_{1d})_{\text{HV}}^{-1}$ are expressed in terms of spectral density functions $J^{(q)}(\omega)$, which themselves are Fourier transforms of the correlation function describing the respective jumping process. The expressions are¹³

$$(T_{1d})_{\text{HH}}^{-1} = \frac{3}{2} C_{\text{HH}} \left(\sum_i r_i^{-6} \right) \{ J^{(1)}(\omega_{\text{H}}) + J^{(2)}(2\omega_{\text{H}}) \} \quad (3)$$

and

$$(T_{1d})_{\text{HV}}^{-1} = C_{\text{HV}} \left(\sum_j r_j^{-6} \right) \left\{ \frac{1}{12} J^{(0)}(\omega_{\text{H}} - \omega_{\text{V}}) + \frac{3}{2} J^{(1)}(\omega_{\text{H}}) + \frac{3}{4} J^{(2)}(\omega_{\text{H}} + \omega_{\text{V}}) \right\}. \quad (4)$$

In the above equations, $C_{\text{HH}} = \gamma_{\text{H}}^4 \hbar^2 I_{\text{H}}(I_{\text{H}} + 1)$ and $C_{\text{HV}} = \gamma_{\text{H}}^2 \gamma_{\text{V}}^2 \hbar^2 S(S + 1)$. ω_{H} and ω_{V} are angular resonance frequencies of ^1H and ^{51}V spins, respectively, γ_{H} and γ_{V} are the gyromagnetic ratios, and r_i and r_j are distances between ^1H spins and between ^1H and ^{51}V spins, respectively. I_{H} and

S are nuclear-spin quantum numbers of ^1H and ^{51}V , which are $\frac{1}{2}$ and $\frac{7}{2}$, respectively. The equations by Bloembergen, Purcell, and Pound (BPP),¹⁴ which are used often to describe hydrogen diffusion in metal hydrides, incorporate assumptions that the motion of diffusing atoms is random and that the dipolar field correlation decays as $\exp(-t/\tau_c)$, τ_c being a correlation time. The spectral density depends on ω and τ_c as

$$J(\omega) \propto \tau_c / (1 + \omega^2 \tau_c^2). \quad (5)$$

Since only ^1H spins are mobile, the mean residence time of the diffusing atom may be denoted as τ_{H} . Then the correlation times between ^1H spins and between ^1H and ^{51}V spins are $\tau_{\text{HH}} = 0.5\tau_{\text{H}}$ and $\tau_{\text{HV}} = \tau_{\text{H}}$, respectively. BPP equations for a cubic lattice are described as

$$(T_{1d})_{\text{HH}}^{-1} = \frac{2}{3} M_{\text{HH}} \left[\frac{0.5\tau_{\text{H}}}{1 + (0.5\omega_{\text{H}}\tau_{\text{H}})^2} + \frac{2\tau_{\text{H}}}{1 + (\omega_{\text{H}}\tau_{\text{H}})^2} \right] \quad (6)$$

and

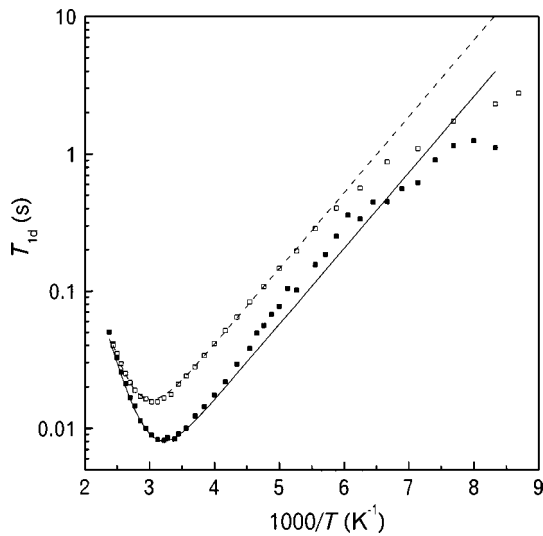


FIG. 8. ^1H spin-lattice relaxation times caused by dipole-dipole interaction in VH_{0.82} at 30.3 (■) and 59.8 MHz (□), and their simulated results indicated by chain and solid lines.

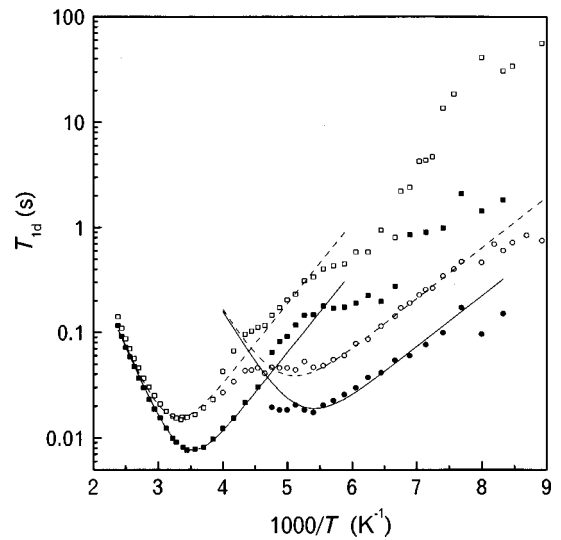


FIG. 9. ^1H spin-lattice relaxation times caused by dipole-dipole interaction in VH_{0.6}D_{0.2} at 30.3 (■, ●) and 59.8 MHz (□, ○), and their simulated results indicated by chain and solid lines.

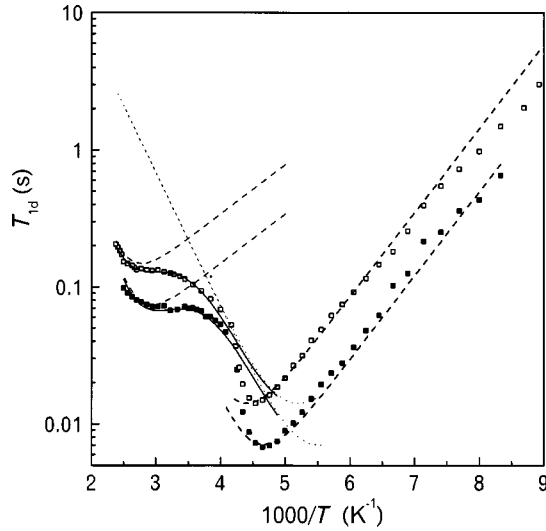


FIG. 10. ^1H spin-lattice relaxation times caused by dipole-dipole interaction in $\text{VH}_{0.2}\text{D}_{0.6}$ at 30.3 (■) and 59.8 MHz (□), and their simulated results indicated by chain and solid lines in the low- and high-temperature ranges, respectively. The chain and dotted lines in the high-temperature range indicate each component.

$$(T_{1d})_{\text{HV}}^{-1} = M_{\text{HV}} \left[\frac{0.5\tau_{\text{H}}}{1 + \{(1 - \gamma_{\text{V}}/\gamma_{\text{H}})\omega_{\text{H}}\tau_{\text{H}}\}^2} + \frac{1.5\tau_{\text{H}}}{1 + (\omega_{\text{H}}\tau_{\text{H}})^2} + \frac{3\tau_{\text{H}}}{1 + \{(1 + \gamma_{\text{V}}/\gamma_{\text{H}})\omega_{\text{H}}\tau_{\text{H}}\}^2} \right]. \quad (7)$$

In the above equations M_{HH} and M_{HV} are the second moments given by

$$M_{\text{HH}} = \frac{3}{5} C_{\text{HH}} \sum_i r_i^{-6} \quad (8)$$

and

$$M_{\text{HV}} = \frac{4}{15} C_{\text{HV}} \sum_j r_j^{-6}. \quad (9)$$

For a thermally activated diffusion process, τ_{H} follows Arrhenius relation, $\tau_{\text{H}} = \tau_{0\text{H}} \exp(E_{\text{H}}/k_{\text{B}}T)$, where $\tau_{0\text{H}}$ is the mean residence time at the infinite temperature or the inverse of a frequency factor, E_{H} is the activation energy, and k_{B} is Boltzmann's constant. Equations (2), (6), and (7) then predict that the plot of T_{1d} versus the inverse of temperature has a minimum, where $\omega_{\text{H}}\tau_{\text{H}} \cong 1$, and that it is symmetric with respect to the minimum position. Moreover, these equations also predict ω_{H}^2 dependence of T_{1d} at low temperatures where $\omega_{\text{H}}\tau_{\text{H}} \gg 1$. At high temperatures where $\omega_{\text{H}}\tau_{\text{H}} \ll 1$, the T_{1d} value is independent of ω_{H} , or the applied magnetic field.

However, it is readily observed in Figs. 8–10 that in no case are the T_{1d} curves symmetric with respect to the minimum position, and also that in every case there is a pronounced deviation from the low temperature ω_{H}^2 proportionality. Such a departure from the so-called BPP-type behavior might be explained by assuming an asymmetric distribution of mean residence times rather than a sharp value of τ_{H} . The above procedure was followed to describe the proton dynamics in $\beta\text{-Ti}_{1-y}\text{V}_y\text{H}_x$,⁹ which might possess a distribution of

nonequivalent positions and potential barriers for the diffusing atoms. There are no good physical reasons to apply such a procedure to VH_x and VH_xD_y alloys. On the other hand, BPP equations have been modified by introducing suitable parameters to adjust the temperature and frequency dependences of T_{1d} .¹⁵ Such modified BPP equations were used to describe the T_{1d} data, the non-BPP behavior of which might be associated with nonisotropic, hindered, or correlated motions.^{15–17} The modification of the spectral density function, Eq. (5), can be written as

$$J(\omega) \propto \Omega^{\beta-1} \tau_c^\beta / [1 + (\omega\tau_c)^{1+\alpha}]. \quad (10)$$

Three additional parameters, α ($0 \leq \alpha \leq 1$), β ($0 \leq \beta \leq 1$), and Ω , are used in the modified $J(\omega)$. In the limit $\alpha \rightarrow 1$ and $\beta \rightarrow 1$, $J(\omega)$ becomes BPP-like. Ω , which is the temperature-independent frequency characteristic of the material, is needed in conjunction with β to give Eq. (10) the correct dimensionality. Ω is of the order of the second moment. Previous uses of such kind of treatment of T_{1d} data revealed that if T_{1d} data have the frequency dependence only in the low-temperature side of the minimum position, as is obtained also if T_{1d} is BPP-like, then only one additional parameter, i.e., α , is sufficient to describe the temperature and frequency dependences of T_{1d} . On the other hand, if T_{1d} exhibits strong frequency dependence in the high-temperature side of the minimum position too, the simulation of T_{1d} data will require the use of both α and β , and consequently Ω .

The equation for $(T_{1d})^{-1}$ then becomes

$$(T_{1d})^{-1} = f_1 \Omega^{\beta-1} \left(\frac{2}{3} M_{\text{HH}} \left[\frac{0.5\tau_{\text{H}}^\beta}{1 + (0.5\omega_{\text{H}}\tau_{\text{H}})^{1+\alpha}} + \frac{2\tau_{\text{H}}^\beta}{1 + (\omega_{\text{H}}\tau_{\text{H}})^{1+\alpha}} \right] + M_{\text{HV}} \left[\frac{0.5\tau_{\text{H}}^\beta}{1 + \{(1 - \gamma_{\text{V}}/\gamma_{\text{H}})\omega_{\text{H}}\tau_{\text{H}}\}^{1+\alpha}} + \frac{1.5\tau_{\text{H}}^\beta}{1 + (\omega_{\text{H}}\tau_{\text{H}})^{1+\alpha}} + \frac{3\tau_{\text{H}}^\beta}{1 + \{(1 + \gamma_{\text{V}}/\gamma_{\text{H}})\omega_{\text{H}}\tau_{\text{H}}\}^{1+\alpha}} \right] \right). \quad (11)$$

The T_{1d} data have been fitted by Eq. (11) and the fitted curves are given in Figs. 8–10 by chain and solid lines. To reduce the number of the adjustable parameters, the $\tau_{0\text{H}}$ values are assumed to be 9×10^{-14} and 3×10^{-14} s for the O and T sites, respectively.⁹ The use of β is not necessary (i.e., β is held at 1) in the present case. In each simulation, M_{HH} and M_{HV} have been calculated theoretically considering that only one type of sites is occupied by all the available H atoms, and the values obtained are listed in Table I. The total ^1H second moment in $\text{VH}_{0.82}$ is 777 kHz^2 , which can be compared with 774 kHz^2 in $\text{VH}_{0.770}$.⁴ It was observed previously that in VH_x systems the T_{1d} calculations using the theoretical second moments led to serious underestimation of T_{1d} minimum,^{4,5,18} and as such it is necessary to incorporate a multiplication factor to the expression of T_{1d} . The factor f_1 in Eq. (11) is adjusted in order to make the minimum of

the simulated curve coincide with the experimental T_{1d} minimum. All the parameters obtained from the fitting procedure are listed in Table II.

The simulated curves change appreciably if the magnitude of either α or E_H is changed by 0.01. The α values range from 0.20–0.55, indicating a significant departure from isotropic diffusion. Alternatively, a kind of correlated motion, in which a jump of one H atom is simultaneous with a jump of another neighboring H atom, may be envisaged.

The f_1 values for the H site showing the main T_1 minimum are between 0.35 and 0.45. The values for the T sites in $\text{VH}_{0.6}\text{D}_{0.2}$ are much small. One tentative reason for the latter is that only a part of the dipolar interaction can contribute to the relaxation due to the restriction of the jumping process. The further small f_1 value for the O' sites in $\text{VH}_{0.2}\text{D}_{0.6}$ means that most of the dipolar interaction is already consumed in the other motions. Explanation of the O' site is described in the next section.

F. Hydrogen sites and diffusion

According to the results shown in Table II and Figs. 8–10, hydrogen sites and diffusion will be discussed for each sample.

In $\text{VH}_{0.82}$, hydrogen atoms occupy the O sites, and they jump between the O sites. The obtained activation energy (E_H) is 0.315 eV/atom. Fukai and Kazama obtained $E_H = 0.29$ eV/atom and $\tau_{0H} = 5 \times 10^{-14}$ s for $\text{VH}_{0.736}$,⁴ though they adopted a treatment much different from the present one to analyze their data. It may be noticed in Fig. 8 that below about 150 K, as the temperature is lowered the T_{1d} data tend to be smaller than the simulated T_{1d} values. If we assume a smaller Korringa constant, the deviation becomes negligible. We however use a high value of Korringa constant estimated from T_1 at 77 K. Similar deviations are obtained for VH_xD_y samples too. There may be other kinds of motions at low temperatures. In the bct phase of the V-H system, there are two kinds of sites in the occupied O sites: O_{z1} and O_{z2} .^{4–6} The hydrogen diffusion between the O_{z2} sites is faster than that between the O_{z1} sites. Accordingly, the deviation at low temperatures might result from the diffusion between the O_{z2} sites.

In $\text{VH}_{0.6}\text{D}_{0.2}$, the high-temperature minimum occurs at a position near to the minimum obtained in $\text{VH}_{0.82}$. $\text{VH}_{0.6}\text{D}_{0.2}$ has a bct structure, and hydrogen atoms occupy predominantly the O sites. The single T_1 above 225 K and the long T_1 component below this temperature (the component 1) correspond to the motion of H atoms in the O sites. The simulation for the component 1 is in good agreement with the experimental data in the temperature range between 160 and 420 K, and yields $E_H = 0.277$ eV/atom. The short T_1 component below 225 K is considered to come from the H atoms occupying the T sites which have higher mobility than the H atoms in the O sites. For the short T_1 component (the component 2), the E_H value is 0.20 eV/atom, which is smaller than that of the component 1. The existence of two components is also observed in the ^1H NMR spectra.

For the longer T_1 component, the T_1 values deviate from the simulated curves below about 160 K. For the V-H systems, the ^1H - ^{51}V dipolar interaction is more effective than the ^1H - ^1H interaction in the ^1H relaxation, as Table I shows.

The H atoms in the O and T sites diffuse independently below 225 K, and their relaxation times may also change with temperature independently. However, at low temperatures when the motion of H atoms in the O sites is sufficiently slow, they might experience an additional relaxation mechanism through spin diffusion from more mobile H atoms in the T sites. It may be noted from the parameters given in Table II that the mean residence time (τ_H) of the octahedral H atoms is 5×10^{-5} s at 160 K while that of the tetrahedral H atoms is 6×10^{-8} s. At high temperatures, there is only one T_1 component, suggesting the occurrence of the exchange of H atoms between the O and T sites.

For $\text{VH}_{0.2}\text{D}_{0.6}$, which is bcc, it would be reasonable to suggest that H atoms occupy mainly the T sites as do the D atoms. H atoms diffuse among the T sites. Below 220 K the simulation of T_{1d} (Fig. 10) yields $E_H = 0.23$ eV/atom. Around 240 K, the H motion in $\text{VH}_{0.2}\text{D}_{0.6}$ undergoes a drastic change following the order-disorder transition of the D sublattice. The H motion above the phase-transition temperature is simulated by assuming that immediately following the transition, only E_H is reduced and that at higher temperatures a new motion is superimposed on the existing motion. The simulated T_{1d} for each of these two components of motion, and the resultant T_{1d} are shown in Fig. 10. The above-mentioned assumptions might be justified because in VH_x the high temperature α'_H phase yields a lower value of activation energy of H motion (about 0.13 eV/atom) than the low-temperature β_H phase,¹⁹ and in the V-H-D systems both the O and T sites could be available to H and D atoms. The new motion at the high temperatures might involve the contribution of the O sites as the diffusion pathway. In this meaning the H site is designated as O' sites.

In the mixed-phase alloy $\text{VH}_{0.4}\text{D}_{0.4}$ (Fig. 7), different H mobilities in the two types of sites led to the observation of two components in the temperature range between 120 and 295 K. The component with the minimum near 215 K corresponds to the tetrahedral H atoms in the bcc phase, and the other component possibly showing a minimum near 270 K arises from the octahedral H atoms in the bct phase. Apparently only one T_1 component exists in the temperature range between 145 and 170 K. A decrease might occur in the T_1 value of the octahedral H atoms in $\text{VH}_{0.4}\text{D}_{0.4}$, similarly to that in $\text{VH}_{0.6}\text{D}_{0.2}$ below about 160 K.

G. ^2H NMR spectra

^2H NMR spectra have been recorded for $\text{VD}_{0.81}$ and VH_xD_y at 30.7 and 61.4 MHz in the temperature range between 140 and 420 K. The ^2H line shapes at various temperatures in $\text{VH}_{0.2}\text{D}_{0.6}$ and $\text{VH}_{0.6}\text{D}_{0.2}$ obtained at 30.7 MHz are shown in Figs. 11 and 12, respectively. $\text{VD}_{0.81}$ and $\text{VH}_{0.4}\text{D}_{0.4}$ show line shapes similar to those of $\text{VH}_{0.2}\text{D}_{0.6}$.

In $\text{VD}_{0.81}$ and $\text{VH}_{0.2}\text{D}_{0.6}$, a narrow resonance line is obtained above 230 K. Below this temperature, the linewidth rapidly increases, and at 220 K the spectra consist of a narrow central component and a doublet having a splitting of about 28 kHz. The doublet pattern arises mainly from ^2H nuclear quadrupole interaction, i.e., the interaction between the ^2H quadrupole moment and the local electric-field gradients (EFG) arising principally from the metal ions. With the lowering of temperature, the central component disappears

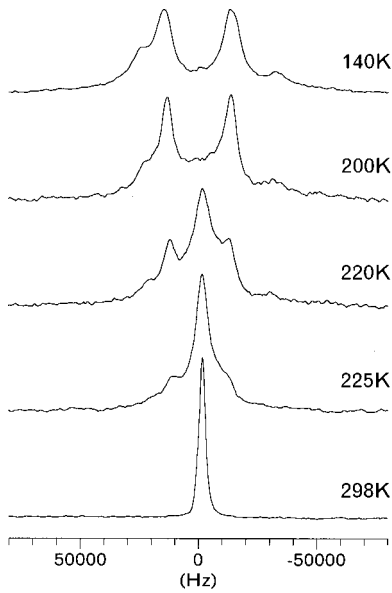


FIG. 11. Temperature dependence of ^2H NMR spectra in $\text{VH}_{0.2}\text{D}_{0.6}$, measured at 30.7 MHz.

below about 210 K, and the peaks on both high- and low-frequency sides of the above-mentioned doublet become apparent.

In $\text{VH}_{0.6}\text{D}_{0.2}$, a narrow resonance line is obtained above 380 K. With decrease in temperature the linewidth increases, and at about 300 K the line is asymmetrically broadened. Further lowering of temperature increases the asymmetry of the line shape, and at 240 K the line shape comprises of a doublet with a peak splitting of about 46 kHz and a central narrow component. The splitting increases gradually, the central component disappears, and in its place there appears another doublet with a splitting smaller than that of the previous one. At 140 K, the ^2H resonance is a superposition of a pair of doublets with splittings of about 56 and 30 kHz.

$\text{VH}_{0.4}\text{D}_{0.4}$, which is a mixed-phase sample of the bcc and bct phases, shows ^2H spectra similar to those of $\text{VH}_{0.2}\text{D}_{0.6}$,

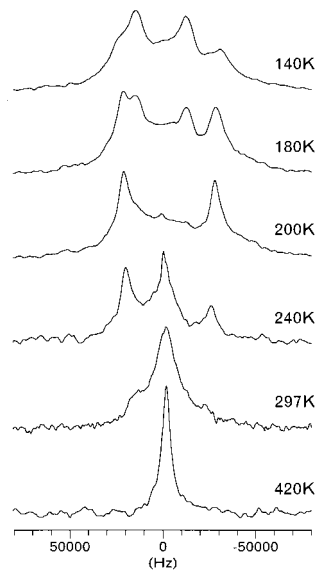


FIG. 12. Temperature dependence of ^2H NMR spectra in $\text{VH}_{0.6}\text{D}_{0.2}$, measured at 30.7 MHz.

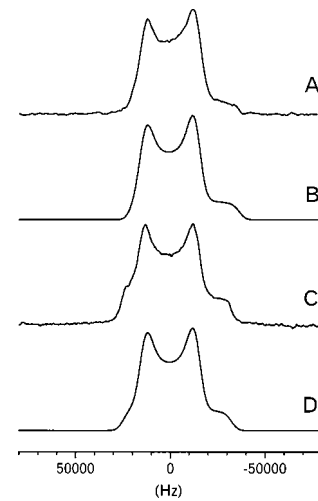


FIG. 13. Simulation of ^2H NMR spectra of $\text{VD}_{0.81}$ at 140 K. The observed spectra at 61.4 (A) and 30.7 MHz (C), and their respective simulated spectra (B and D).

indicating that the contribution of the bcc phase is much larger than that of the bct phase.

The ^2H line shape depends markedly on instrumental conditions; the 90° pulse width, rf pulse homogeneity across the sample volume, the pulse interval τ_1 , and the setting of τ_2 on the echo maximum. In the spectra shown in Figs. 11 and 12, the peaks and shoulders are enhanced accidentally due to the instrumental conditions, leading to magnification of the spectral changes. Figures 13 and 14 shows some ^2H spectra nearer to the true line shapes, which will be used to estimate NMR parameters.

The spectra at 140 K, the lowest temperature studied, are used to evaluate NMR parameters for each site. The simulation is performed with consideration of ^2H quadrupole and Knight shift interactions simultaneously. The quadrupole interaction is described by a quadrupole coupling constant ($\text{QCC} = e^2Qq/h$) and an asymmetric factor of the electric-field gradients (η_Q). Principal values of Knight shift tensor, K_1 , K_2 , and K_3 , are defined as $|K_2 - K_{\text{iso}}| \leq |K_1 - K_{\text{iso}}| \leq |K_3 - K_{\text{iso}}|$, where K_{iso} is isotropic Knight shift [K_{iso}

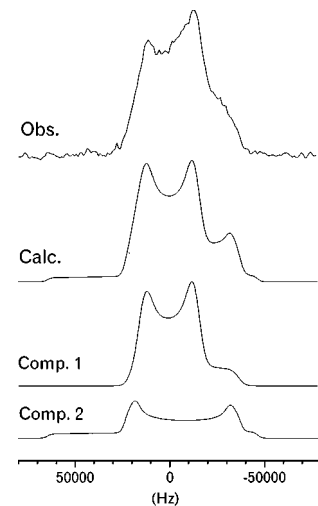


FIG. 14. Simulation of ^2H NMR spectra of $\text{VH}_{0.6}\text{D}_{0.2}$, measured at 61.4 MHz and 140 K.

$= (K_1 + K_2 + K_3)/3$]. The magnitude of Knight shift anisotropy is $\Delta K = K_3 - (K_1 + K_2)/2$, and the asymmetry factor is $\eta_K = (K_2 - K_1)/(K_3 - K_{\text{iso}})$. The relative orientation of the two interactions can be defined by three Euler angles. To reduce the number of the fitting parameters we assume that $\eta_K = 0$ and that Euler angles relating the principal axis systems of the two interactions are all zero. Figure 13 shows the spectra of $\text{VD}_{0.81}$ at 140 K and their simulated spectra. The two spectra measured at 61.4 and 30.7 MHz are simulated simultaneously using the same adjustable parameters. The spectra consist of only one component, which parameters are as follows; $\text{QCC} = 38$ kHz, $\eta_Q = 0.1$, $K_{\text{iso}} = -41$ ppm from D_2O and $\Delta K = -130$ ppm. The spectra of $\text{VH}_{0.2}\text{D}_{0.6}$ at 140 K can be simulated by the same parameters as those of $\text{VD}_{0.81}$. On the other hand, the spectra of $\text{VH}_{0.6}\text{D}_{0.2}$ at 140 K consist of at least two components. Component 1 is assumed to have the same parameters as those in $\text{VD}_{0.81}$ and $\text{VH}_{0.2}\text{D}_{0.6}$. The parameters of component 2 are estimated first from the spectra at 200 K, and then adjusted using the spectra at 140 K. Two spectra at 61.4 and 30.7 MHz are simulated simultaneously, though only the results at 61.4 MHz are shown in Fig. 14. The obtained parameters for the component 2 are $\text{QCC} = 74$ kHz, $\eta_Q = 0.1$, $K_{\text{iso}} = -24$ ppm from D_2O and $\Delta K = 260$ ppm. At 200 K, QCC reduces to 62 kHz. The intensity ratio of the component 1 to the component 2 is 2 ± 1 . The spectra of $\text{VH}_{0.4}\text{D}_{0.4}$ at 140 K can be simulated by only the component 1, and the contribution of the component 2 is not confirmed, although this sample contains the bct phase.

Thus two types of sites in VH_xD_y can be distinguished by ^2H NMR, which have quadrupole and Knight shift interactions different from each other. Salibi *et al.* presented ^2H NMR spectra for $\text{VD}_{0.59}$ in the $(\alpha_D + \beta_D)$ mixed phase at 244 K and the $(\beta_D + \delta_D)$ mixed phase at 194 K.⁸ They obtained a narrow line for the α phase in which D atoms occupy mostly the T sites, a doublet with 53 kHz splitting for octahedral D atoms in the β_D phase, and a doublet with 27 kHz splitting for tetrahedral D atoms in the δ_D phase. The V-D phase diagram¹ shows that $\text{VD}_{0.81}$, which has a bcc structure in the temperature range between 140 and 420 K, is in the α_D phase above about 230 K and in the δ_D phase below this temperature. Accordingly, in the present samples of VH_xD_y and $\text{VD}_{0.81}$, the doublet with the smaller splitting ($\text{QCC} = 38$ kHz) can be ascribed to D atoms in the T sites, and that with the larger splitting ($\text{QCC} = 74$ kHz) to D atoms in the O sites.

The temperature dependence of the line shape reflects deuterium motions. In $\text{VD}_{0.81}$ and $\text{VH}_{0.2}\text{D}_{0.6}$, D atoms occupy the ordered T sites at low temperatures, and the ordering remains up to about 200 K. The ordered D sublattice collapses by the phase transition from the δ_D phase to the α_D phase, accompanied by the growth of the narrow central line. After the phase transition, the doublet disappears, and only the narrow central line is observed reflecting the isotropic diffusion of D atoms.

In $\text{VH}_{0.6}\text{D}_{0.2}$, in which the host metal lattice is bct, D atoms occupy both the O and T sites of comparable magnitudes. With increase in temperature, first the inner doublet corresponding to the T sites disappears at about 200 K, and then the narrow central component grows up. The outer doublet corresponding to the O sites remains up to about 240 K.

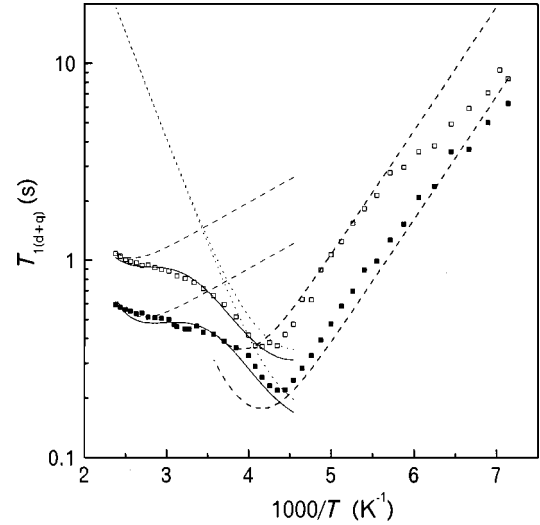


FIG. 15. ^2H spin-lattice relaxation times caused by dipole-dipole and/or quadrupole interaction in $\text{VD}_{0.81}$ at 30.7 MHz (■) and 61.4 MHz (□), and their simulated results indicated by chain and solid lines in the low- and high-temperature ranges, respectively. The chain and dotted lines in the high-temperature range indicate each component.

Above 240 K, the doublet peak disappears, though the asymmetric line shape is observed up to about 380 K. These results demonstrate that the D atoms in the T site have higher mobility than D in the O sites. The diffusion of D atoms in the O sites becomes isotropic above 380 K, much higher than that in the T sites (about 200 K). These results are consistent with the ^1H NMR results.

H. ^2H spin-lattice relaxation time

^2H spin-lattice relaxation times T_1 have been measured at 30.7 and 61.4 MHz in the temperature range between 140 and 420 K. The T_1 values are determined from the recovery of peak amplitudes in the spectra. In $\text{VD}_{0.81}$ and $\text{VH}_{0.2}\text{D}_{0.6}$ there is a narrow peak above 230 K. At low temperatures, the quadrupolar splitting corresponding to D atoms in the T sites is prominent, and the recovery of one of the doublet peaks is measured. The recoveries are exponential at all the temperatures studied. The spin-lattice relaxation times after subtracting the contribution of conduction electrons are plotted in Figs. 15 and 16 as a function of inverse temperature. The subtraction procedures will be described in the next section. The values have their minimum values around 230 K probably because of the phase transition from the δ_D phase to the α_D phase. The minimum values are 0.22 s (at 230 K) and 0.36 s (240 K) at 30.7 and 61.4 MHz, respectively, for $\text{VD}_{0.81}$. They are 0.24 s (220 K) and 0.38 s (230 K), respectively, for $\text{VH}_{0.2}\text{D}_{0.6}$. The T_1 versus T^{-1} plots show a large asymmetry with respect to the minimum position. The temperature dependences are similar to those of ^1H T_1 for the same samples.

In $\text{VH}_{0.6}\text{D}_{0.2}$, the spectra have many peaks depending on the sample temperature, as shown in Fig. 12. Below about 250 K, the amplitude of the central narrow component or that of either of the two peaks of the doublet corresponding to the octahedral D atoms is plotted as a function of time, and the recovery is found to be nonexponential. The peak amplitudes of the doublets corresponding to both the O and T sites are

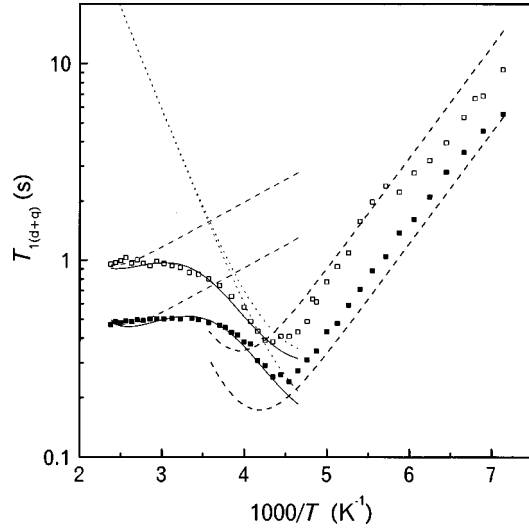


FIG. 16. ^2H spin-lattice relaxation times caused by dipole-dipole and/or quadrupole interaction in $\text{VH}_{0.2}\text{D}_{0.6}$ at 30.7 MHz (■) and 61.4 MHz (□), and their simulated results indicated by chain and solid lines in the low- and high-temperature ranges, respectively. The chain and dotted lines in the high-temperature range indicate each component.

monitored below 190 K, and the recoveries are nonexponential in both sites. However, the apparent characteristic time of recovery for the peak corresponding to D atoms in the O site is found to be longer than that corresponding to D atoms in the T site. Below 250 K, the recovery curves are analyzed as a sum of two exponents with different magnitudes and characteristic times. In accordance with the above-mentioned observation, the longer characteristic time is denoted as T_1 of D atoms in the O sites, and the shorter one as T_1 of D atoms in the T sites. Above 250 K the recovery curves are exponential. This exponential behavior might indicate that the two types of sites become equivalent at high temperatures in regard to the deuterium motion. In other words, D atoms in the O and T sites are exchanged mutually. The obtained T_1 values are plotted in Fig. 17. There is a minimum value of 0.12 s at 340 K when measured at 30.7 MHz, while the minimum at 61.4 MHz is considered to locate above 370 K. By analogy with ^1H T_1 in $\text{VH}_{0.6}\text{D}_{0.2}$, the ^2H T_1 values above 250 K reflect the D motion in the O site dominantly. Therefore the same marks are used in the figure for the longer T_1 component below 250 K and the single T_1 above 250 K.

I. Analysis of ^2H spin-lattice relaxation time

The ^2H spin-lattice relaxation time in the present systems is expressed as

$$(T_1)^{-1} = (T_{1d})^{-1} + (T_{1q})^{-1} + (T_{1e})^{-1}, \quad (12)$$

where $(T_{1d})^{-1}$ is contribution from modulation of nuclear dipolar interactions, $(T_{1q})^{-1}$ is contribution due to fluctuation of ^2H quadrupole interaction, and $(T_{1e})^{-1}$ arises from fluctuation of hyperfine interaction between the nuclear spin and conduction electrons. The contribution from paramagnetic impurities is ignored as in the case of ^1H T_1 . For VH_xD_y samples, ^2H Korringa constants ($T_{1e}T$) are the respective ^1H Korringa constant multiplied by 42.44

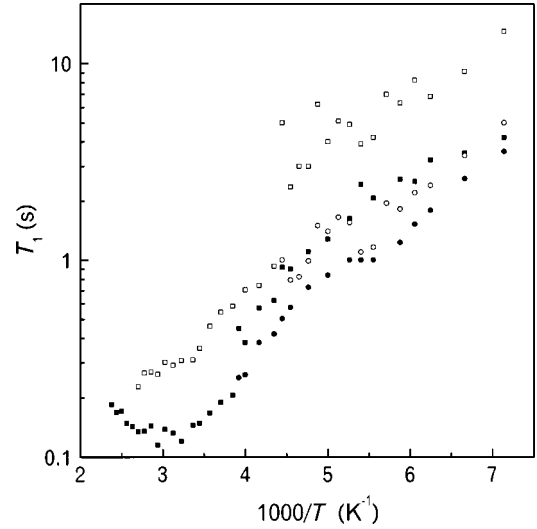


FIG. 17. Temperature dependences of ^2H spin-lattice relaxation times in $\text{VH}_{0.6}\text{D}_{0.2}$. ■: The O site at 30.7 MHz, □: the O site at 61.4 MHz, ●: the T site at 30.7 MHz, and ○: the T site at 61.4 MHz.

($= \gamma_{\text{H}}^2 / \gamma_{\text{D}}^2$). For $\text{VD}_{0.81}$, the ^2H Korringa constant is assumed to be same as that of $\text{VH}_{0.2}\text{D}_{0.6}$. They are listed in Table III. Contribution of $(T_{1e})^{-1}$ is subtracted using Korringa relation, although the contribution is very small in the temperature range studied.

In the ^2H dipolar relaxation rate, $(T_{1d})^{-1}$, of the VD_y and VH_xD_y systems ^2H - ^2H and ^2H - ^1H interactions have a negligible contribution compared to ^2H - ^{51}V interaction because of the low gyromagnetic ratio of ^2H . The T_{1d} for ^2H can be described as follows, taking into account the ^2H - ^{51}V dipolar interaction only:

$$(T_{1d})^{-1} = f_1 \Omega^{\beta-1} M_{\text{DV}} \left[\frac{0.5 \tau_{\text{D}}^{\beta}}{1 + \{(1 - \gamma_{\text{V}} / \gamma_{\text{D}}) \omega_{\text{D}} \tau_{\text{D}}\}^{1+\alpha}} + \frac{1.5 \tau_{\text{D}}^{\beta}}{1 + (\omega_{\text{D}} \tau_{\text{D}})^{1+\alpha}} + \frac{3 \tau_{\text{D}}^{\beta}}{1 + \{(1 + \gamma_{\text{V}} / \gamma_{\text{D}}) \omega_{\text{D}} \tau_{\text{D}}\}^{1+\alpha}} \right]. \quad (13)$$

ω_{D} , γ_{D} , and τ_{D} are the angular resonance frequency, the gyromagnetic ratio, and the mean residence time of ^2H . M_{DV} is the second moment caused by the ^2H - ^{51}V dipolar interaction, which is written as

$$M_{\text{DV}} = \frac{4}{15} C_{\text{DV}} \sum_k r_k^{-6}, \quad (14)$$

where $C_{\text{DV}} = \gamma_{\text{D}}^2 \gamma_{\text{V}}^2 \hbar^2 S(S+1)$ and r_k is a distance between ^2H and ^{51}V spins.

The BPP-type equation for the quadrupolar relaxation is described as¹³

$$(T_{1q})^{-1} = \frac{3}{40} \left(\frac{e^2 Q q}{\hbar} \right)^2 \left(1 + \frac{\eta_Q^2}{3} \right) \left[\frac{\tau_{\text{D}}}{1 + (\omega_{\text{D}} \tau_{\text{D}})^2} + \frac{4 \tau_{\text{D}}}{1 + (2 \omega_{\text{D}} \tau_{\text{D}})^2} \right]. \quad (15)$$

TABLE III. ^2H Korringa constants and parameters of deuterium diffusion.

Sample	$T_{1e}T^a$ (s K)	D site	τ_{0D}^b (s)	E_D (eV/atom)	α	f_1
VH _{0.6} D _{0.2}	7720	<i>O</i>	13×10^{-14}	0.33	0.35	1.60
VH _{0.2} D _{0.6}	8660	<i>T</i> ^c	4.2×10^{-14}	0.25	0.45	1.15
		<i>T</i> ^d	4.2×10^{-14}	0.205	0.45 ^e	1.15 ^e
		<i>O'</i> ^d	13×10^{-14}	0.42	0.11	0.30
VD _{0.81}	8660 ^f	<i>T</i> ^c	4.2×10^{-14}	0.25	0.50	1.15
		<i>T</i> ^d	4.2×10^{-14}	0.215	0.50 ^e	1.15 ^e
		<i>O'</i> ^d	13×10^{-14}	0.39	0.12	0.28

^aEstimated from ^1H Korringa constants.

^bAssumed to be $1.4\tau_{0H}$ (Ref. 10).

^cBelow 220 K.

^dAbove 240 K.

^eAssumed.

^fAssumed to be the same as that in VH_{0.2}D_{0.6}.

When the spectral density function in Eq. (10) is used, the $(T_{1q})^{-1}$ is described as

$$(T_{1q})^{-1} = f_2 \Omega^{\beta-1} \frac{3}{40} \left(\frac{e^2 Q q}{\hbar} \right)^2 \left(1 + \frac{\eta_Q^2}{3} \right) \left[\frac{\tau_D^\beta}{1 + (\omega_D \tau_D)^{1+\alpha}} + \frac{4\tau_D^\beta}{1 + (2\omega_D \tau_D)^{1+\alpha}} \right]. \quad (16)$$

f_2 is a multiplication factor similar to f_1 .

Since the dipolar relaxations in both ^1H and ^2H spins are dominated by the dipolar interaction with ^{51}V spins, the relaxation rates scale roughly as γ_H^2/γ_D^2 . For example, the ^1H T_1 minimum of 6.7 ms (at 215 K and 30.3 MHz) in VH_{0.2}D_{0.6} corresponds to ^2H T_1 of 0.28 s. The experimental ^2H T_1 at 215 K is 0.27 s at 30.7 MHz. Another example is that the ^1H T_1 minimum of 7.7 ms (at 280 K and 30.3 MHz) in VH_{0.6}D_{0.2} corresponds to ^2H T_1 of 0.33 s. The experimental ^2H T_1 minimum in VH_{0.6}D_{0.2} is 0.12 s (340 K) at 30.7 MHz. The above and similar simple comparisons between the scaled ^1H T_{1d} and the experimental ^2H T_1 show that the dipolar interaction has an overwhelming effect in causing ^2H spin-lattice relaxation in VH_{0.2}D_{0.6} and VD_{0.81}, and that the quadrupole interaction has considerable contributions in VH_{0.6}D_{0.2}.

If the quadrupole interaction contributes to the ^2H relaxation, the expected T_{1q} minimum values estimated from Eq. (15) by assuming $\omega_D \tau_D \approx 1$ are 63 and 17 ms for the *T* and *O* sites, respectively, at 30.7 MHz. These values are much smaller than the T_1 minimum values experimentally obtained. Therefore even if the quadrupole interaction contributes to the relaxation, only a small part of it contributes.

After removing the contribution of conduction electrons, the relaxation time includes the contributions from the dipolar interaction and the quadrupole interaction, which is denoted as $T_{1(d+q)}$. The quadrupolar relaxation shows temperature and frequency dependences similar to those of the dipolar relaxation. Tentatively, only the dipolar relaxation described by Eq. (13) is taken into account in the simulation.

The multiplication factor f_1 reflects the contribution from the quadrupole interaction. The simulated results are shown in Figs. 15, 16, and 18 by chain and solid lines. Similarly to the ^1H T_1 analysis, the τ_{0D} values are assumed to be 13×10^{-14} and 4.2×10^{-14} s for the *O* and *T* sites, respectively, from the relation that $\tau_{0D} = 1.4\tau_{0H}$.¹⁰ The fittings are quite satisfactory. All the results, viz., the activation energies E_D , the α values and the multiplication factors f_1 thus obtained are given in Table III. In all these simulations, β is 1 as it is in case of the H motion. The f_1 values are less than 0.5 in ^1H T_1 , whereas they are more than 1 in ^2H T_1 except for the overlapping motion in the high-temperature range, suggesting the contribution of the quadrupole interaction to the relaxation.

J. Deuterium sites and diffusion

In VD_{0.81} and VH_{0.2}D_{0.6}, the D atoms occupy the *T* sites, and jump among the ordered *T* sites in the δ_D phase. Hop-

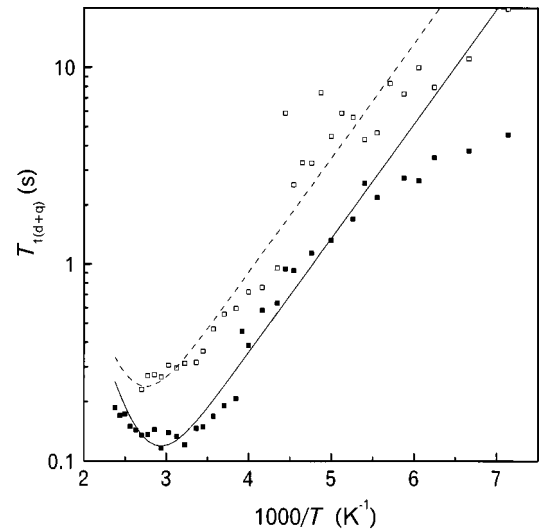


FIG. 18. ^2H spin-lattice relaxation times caused by dipole-dipole and/or quadrupole interaction in VH_{0.6}D_{0.2} (the *O* site) at 30.7 (■) and 61.4 MHz (□), and their simulated results indicated by chain and solid lines.

ping among the ordered T sites does neither average out the structured quadrupolar line shape, nor does it produce effective quadrupolar spin-lattice relaxation. The simulation yields $E_H = 0.25$ eV/atom below 220 K. Above 230 K in the α_D phase, where the deuterium sublattice becomes disordered, there might be considerable quadrupolar relaxation of ^2H , since the quadrupolar line shape collapses. The deuterium diffusion changes drastically around the phase-transition temperature. By analogy with the H motion in $\text{VH}_{0.2}\text{D}_{0.6}$, the D motion above the phase-transition temperature is simulated by assuming that immediately following the transition, only E_D is reduced and that at higher temperatures a new motion is superimposed on the existing motion. The new D motion is considered to be similar to the H motion at the high temperatures which might involve the contribution of the O sites as the diffusion pathway.

In case of $\text{VH}_{0.6}\text{D}_{0.2}$, ^2H spectra confirm the existence of D atoms in two kinds of sites, the O and T sites. For the O sites, the effective quadrupole coupling constant gradually decreases with temperature, and the quadrupolar structure of the O sites begins to destroy at about 230 K. The quadrupolar line shape disappears at about 380 K. The obtained f_1 value (1.60) demonstrates that the quadrupole interaction contributes to the relaxation as well as the dipolar interaction between the ^2H and ^{51}V spins does. In the bct structure, the D atoms occupy the O_z sites. Hopping among the O_z sites preserves the quadrupole line shape. The collapse of the quadrupole pattern suggests that sites other than the O_z sites, i.e., O_x , O_y , and/or T sites are also used for the D diffusion. It has been observed that in tantalum, niobium, and vanadium deuterides, the hopping among the ordered sites produces the dipolar relaxation, while maintaining the quadrupolar structured line shape.⁸ In the low-temperature region, the observed T_1 values for the O sites deviates from the simulated lines, which might be caused by the mechanism similar to the ^1H T_1 case.

The D atoms in the T sites diffuse faster than those in the O sites at low temperatures for $\text{VH}_{0.6}\text{D}_{0.2}$, which is confirmed by both ^2H NMR spectra and ^2H T_1 . The D atoms in the T sites form an ordered sublattice in the bct structure below the lowest temperature studied. The ordering gradually degrades with increase in temperature, as the DSC curve shows. The quadrupolar line shape disappears at about 200 K, indicating the disordered arrangement and diffusion of the D atoms. The dipolar relaxation seems to be dominant below 200 K, while the quadrupolar relaxation might be dominant above 200 K. Due to the scattering of the observed T_1 data and complexity of the relaxation mechanisms, parameters of the D diffusion could not be estimated for the T sites.

K. Comparison between hydrogen and deuterium

The site and diffusion are compared between H and D atoms in the V-H-D system. For $\text{VH}_{0.81}$, H atoms occupy the O sites in the bct structure. In the hydrogen-rich $\text{VH}_{0.6}\text{D}_{0.2}$, which is also bct, H and D atoms occupy both the O and T sites. For the deuterium-rich $\text{VH}_{0.2}\text{D}_{0.6}$ and $\text{VD}_{0.81}$ H and D atoms occupy the T sites in the bcc lattice. In the mixed-phase $\text{VH}_{0.4}\text{D}_{0.4}$, H atoms occupy both the O and T sites, while D atoms occupy predominantly the T sites.

In the bct phase, the H and D atoms in the T sites diffuses faster than those in the O sites. For the T sites, the H diffusion in the bct phase is faster than that in the bcc ordered phase, and is comparable with that in the bcc disordered phase. If the phase and the site are both specified, the H atoms always diffuse faster than D.

Comparison between $\text{VH}_{0.82}$ and $\text{VH}_{0.6}\text{D}_{0.2}$ indicates that introduction of D into the V-H system leads to decrease in the activation energy of H diffusion in the O sites and to increases the occupancy of the T sites, both resulting in the higher mobility of H atoms. On the other hand, comparison between $\text{VD}_{0.81}$ and $\text{VH}_{0.2}\text{D}_{0.6}$ indicates that introduction of H into the V-D system does not influence the D site occupancy, resulting in little change in the D mobility.

IV. CONCLUSION

Vanadium-hydrogen-deuterium (V-H-D) alloys with $([\text{H}] + [\text{D}]) / [\text{V}] = 0.8$ have been studied by means of x-ray diffraction (XRD), DSC, and ^1H and ^2H NMR and the following conclusions have been obtained.

(i) The crystal structures of $\text{VH}_{0.82}$ and $\text{VH}_{0.6}\text{D}_{0.2}$ are bct at room temperature, while those of $\text{VH}_{0.2}\text{D}_{0.6}$ and $\text{VD}_{0.81}$ are bcc. $\text{VH}_{0.4}\text{D}_{0.4}$ is in a mixed phase of bct and bcc, demonstrating that there exists an immiscibility gap.

(ii) The phase transition from the δ_D phase to the α_D phase is observed in $\text{VD}_{0.81}$ between 200 and 240 K by DSC. The transition temperature range becomes broadened and shifted toward the lower temperature as the $[\text{H}]/[\text{D}]$ ratio increases. In $\text{VH}_{0.82}$ no phase transition is observed in the temperature range between 120 and 295 K.

(iii) In $\text{VH}_{0.82}$ H atoms occupy the O sites, and H diffusion takes place between the ordered O sites, leaving residual dipolar broadening. In $\text{VH}_{0.6}\text{D}_{0.2}$, H and D atoms occupy both the O and T sites, and the H and D atoms in the T sites diffuse faster than those in the O sites. The diffusion between the ordered O sites is confirmed by the ^1H residual dipolar broadening and by the ^2H quadrupolar line shape.

(iv) In $\text{VH}_{0.2}\text{D}_{0.6}$ and $\text{VD}_{0.81}$ H and D atoms occupy the T sites. In the δ_D phase H and D atoms diffuse among the ordered T sites, the ^2H quadrupolar line shape is preserved, and the ^2H relaxation is dominated by the dipolar interaction. Around the phase transition temperature, the diffusion changes drastically. In the α_D phase the diffusion takes place between the disordered T sites, and another motional mode takes place simultaneously.

(v) The temperature and frequency dependences of T_1 of ^1H and ^2H can be described by modified Bloembergen-Purcell-Pound equations, suggesting that H and D atoms undergo some kind of correlated motions.

ACKNOWLEDGMENTS

The authors are grateful to Dr. E. Akiba of our institute for help in measuring the x-ray powder diffraction. B.B. wishes to acknowledge the Science and Technology Agency of Japan for financial assistance.

- *Present address: Saha Institute of Nuclear Physics, Calcutta 700 064, India.
- †Author to whom correspondence should be addressed. Electronic address: hayashi@nimc.go.jp
- ¹B. Siegel and G. G. Libowitz, in *Metal Hydrides*, edited by W. M. Mueller, J. P. Blackledge, and G. G. Libowitz (Academic, New York, 1968), p. 592.
- ²T. Shober and H. Wenzl, in *Hydrogen in Metals II*, edited by G. Alefeld and J. Völkl (Springer-Verlag, Berlin, 1978), p. 11.
- ³R. M. Cotts, in *Hydrogen in Metals I*, edited by G. Alefeld and J. Völkl (Springer-Verlag, Berlin, 1978), p. 227.
- ⁴Y. Fukai and S. Kazama, *Acta Metall.* **25**, 59 (1977).
- ⁵S. Hayashi, K. Hayamizu, and O. Yamamoto, *J. Chem. Phys.* **76**, 4392 (1982).
- ⁶S. Hayashi, K. Hayamizu, and O. Yamamoto, *J. Chem. Phys.* **77**, 2210 (1982).
- ⁷J. Völkl and G. Alefeld, in *Hydrogen in Metals I* (Ref. 3), p. 321.
- ⁸N. Salibi, B. Ting, D. Cornell, and R. E. Norberg, *Phys. Rev. B* **38**, 4416 (1988).
- ⁹T. Ueda and S. Hayashi, *J. Alloys Compd.* **231**, 226 (1995).
- ¹⁰T. Ueda and S. Hayashi, *J. Alloys Compd.* **256**, 145 (1997).
- ¹¹Y. Fukai, K. Kubo, and S. Kazama, *Z. Phys. Chem., Neue Folge* **115**, 245 (1979).
- ¹²S. Kazama and Y. Fukai, *J. Phys. Soc. Jpn.* **42**, 119 (1977).
- ¹³A. Abragam, *The Principles of Nuclear Magnetism* (Oxford University Press, London, 1961).
- ¹⁴N. Bloembergen, E. M. Purcell, and R. V. Pound, *Phys. Rev.* **73**, 679 (1948).
- ¹⁵T. C. Jones, T. K. Halstead, and K. H. J. Buschow, *J. Less-Common Met.* **73**, 209 (1980).
- ¹⁶T. K. Halstead, K. Metcalfe, and T. C. Jones, *J. Magn. Reson.* **47**, 292 (1982).
- ¹⁷Cl. Ritter, W. Muller-Warmuth, and R. Schollhorn, *J. Chem. Phys.* **83**, 6130 (1985).
- ¹⁸S. Hayashi, K. Hayamizu, and O. Yamamoto, *J. Chem. Phys.* **78**, 5096 (1983).
- ¹⁹J. E. Kleiner, E. H. Sevilla, and R. M. Cotts, *Phys. Rev. B* **33**, 6662 (1986).